The 9th European Congress on Computational Methods in Applied Sciences and Engineering
ECCOMAS Congress 2024
3–7 June 2024, Lisboa, Portugal

MAPPING MANUFACTURING VARIABILITY TO COMPOSITE PRESSURE VESSELS' GEOMETRY

Rafael Santos[1, 2, 3], **Augustin Persoons**[1, 3] **and David Moens**[1, 3]

[1] Department of Mechanical Engineering Division LMSD, KU Leuven
Sint-Katelijne-Waver, Antwerp 2860, Belgium

[2] SIM vzw Technologiepark 935, BE-9052, Zwijnaarde, Belgium

[3] Flanders Make@KU Leuven
e-mail: rafael.santos@kuleuven.be

Key words: Composite Pressure Vessels, Filament Winding, Composites, Uncertainty Quantification, Energy Storage, Hydrogen

Summary. In the context of vehicles powered by hydrogen fuel cells, hydrogen is stored as a compressed gas within tanks constructed from carbon fiber composites. These tanks are engineered with a margin of safety set at 2.25 times the nominal working pressure. Showing a minimal variability in the tank's strength will allow for a decrease in this margin of safety. This can be accomplished by predicting both the vessel's strength and its associated uncertainties. In this work, several composite pressure vessels (CPVs) were manufactured through wet fiber winding, and the parameters that control the winding were recorded as time signals. Some of these parameters include used fiber length, fiber tension, winding speed, liner pressure and fiber volume fraction. The winding process is controlled by an algorithm that follows winding paths based on a defined winding angle and number of circuits around the vessel. These paths are defined by Euclidean and cylindrical coordinates that can be used to calculate the amount of fiber used between each coordinate. This obtained fiber used is then matched to the fiber used signal recorded during winding in order to match the recorded signals to the winding paths. This allows the parameters to be mapped to the geometry of the vessel. Afterwards, Gaussian Process Regression (Kriging) is used to obtain random fields over the geometry of the vessel for each manufacturing parameter of interest. This allows to identify and visualize the distribution of these parameters over the geometry of the vessel and potentially identify areas of the vessel where failure is more likely to start.

1 INTRODUCTION

Pressure vessels are crucial in various industries such as aerospace, automotive, energy, and chemicals, where safely storing and transporting pressurized liquids or gases is of high importance. Historically, metallic materials like steel and aluminum have been used due to their mechanical properties, proven track record, and relative low cost [5, 12].

However, metal pressure vessels present disadvantages, such as high weight, corrosion, and limited lifespan due to fatigue. These issues have driven research into alternative materials, with fiber-reinforced composites emerging as a promising alternative. Filament winding, a manufacturing process that became prominent in the 1980s and 1990s, is widely used for creating

composite pressure vessels (CPVs), which are increasingly used across industries. CPVs offer remarkable strength, relative low weight, and corrosion resistance, making them ideal for storing and transporting pressurized fluids [5].

CPVs are produced using techniques such as filament winding, tape laying, and automated fiber placement, which allow precise fiber deposition to optimize strength and stiffness. High-performance fibers like carbon and aramid further enhance the vessels' mechanical properties [5].

The burst pressure performance of CPVs is critical, as they often contain flammable or highly reactive fluids. Safety and standardization of these vessels are regulated by bodies like the American Society of Mechanical Engineers (ASME) and the US Department of Transportation (DOT), which set guidelines for design, manufacturing, testing, and certification. A key aspect of CPV design is the margin of safety, ensuring the vessel can withstand maximum operating pressures influenced by factors like temperature fluctuations and impacts. ASME's Boiler and Pressure Vessel Code (BPVC) Section X stipulates that burst pressure for glass and carbon fiber-reinforced CPVs must be at least 3.5 and 2.25 times the design pressure, respectively [5, 12, 8, 2].

Reducing the safety margin in CPV design can yield significant economic and environmental benefits. A smaller safety margin reduces vessel size and weight, lowering material and manufacturing costs and decreasing the carbon footprint. However, this reduction must not compromise safety. The safety margin must account for uncertainties in materials, design, and loading conditions. To safely reduce the safety margin, it is essential to accurately predict the vessel's burst strength considering manufacturing conditions and their uncertainties [12, 10].

Filament-wound CPVs are characterized by both design and process parameters, such as fiber tension, winding speed, winding angle, fiber volume fraction, and liner pressure. The manufacturing process also includes curing, where additional parameters like internal pressure and temperature cycle are controlled [1].

Finite element analysis (FEA) is one method to predict CPV burst strength, though it presents limitations [10, 9, 3, 4, 7, 6]. FEA requires assumptions and simplifications that may not fully represent empirical data. Additionally, including parameters like tow tension and winding speed in traditional FEA is not straightforward.

Alternatively, black-box modeling uses machine learning (ML) algorithms to identify relationships between inputs and outputs without access to physical models. For burst strength prediction, known vessel properties and recorded manufacturing conditions can train ML algorithms against experimental burst data. While this approach requires fewer assumptions, it lacks transparency and demands extensive experimental data, which is costly.

Furthermore, some ML algorithms include explicit ways to model and propagate uncertainty information from the input data to the output. This can help with more accurately predicting the burst pressure of CPVs by quantifying the uncertainty observed in the manufacturing parameters.

Few studies have applied ML to CPV manufacturing. Zolfaghari and Izadi [13] used neural networks to predict the burst pressure of metal vessels, outperforming several analytical models. However, such studies are limited, particularly for composite vessels, where the resulting structure is more complex due to the interaction between fibers and the matrix material.

With this paper, we aim at providing a method to encode the uncertainty in the manufacturing process of CPVs as a first step to produce inputs with uncertainty information. These

then could be used for ML algorithms that predict the burst pressure of these vessels.

We first detail the manufacturing process and data acquisition methods used to produce CPVs. Then we present the methodology for mapping the manufacturing parameters to the vessel geometry and performing Gaussian Process Regression to generate the corresponding fields over the vessel. Finally, we discuss the results of the manufacturing parameter mapping and uncertainty quantification.

2 VESSEL MANUFACTURING AND DATA ACQUISITION

The vessels are produced in an assembly line designed for industrial-scale vessel manufacturing, without adherence to laboratory conditions, therefore these vessels are representative of industry conditions. The manufacturing process involves wet winding of carbon fiber around a polyamide 6 liner with a specified layup comprising hoop and helical layers. The exact layup details are not disclosed due to commercial confidentiality. Each vessel has a uniform nominal laminate thickness of 11.4 mm and outside liner dimensions of 304.6 by 140 mm (Figure 1). Key parameters such as tow tension, liner pressure, winding speed, fiber length used, and winding time are monitored during the winding process.

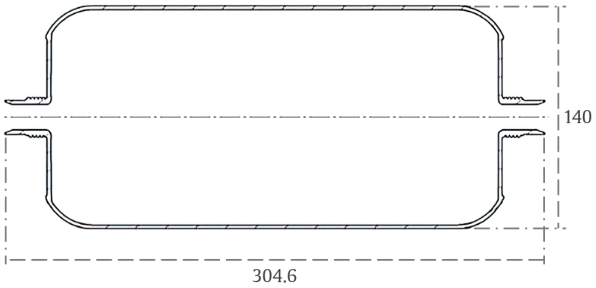

Figure 1: Schematic view of the vessel's liner and liner dimensions. Dimensions in mm.

In this work the variables of interest are the tow tension and winding speed. Therefore five configurations are defined in a design of experiments (DOE) where a baseline configuration with nominal values is defined, and six other configuration where the variables of interest are varied. This design of experiment can be found in Table 1.

Table 1: Design of experiments. Nominal values are omitted due to commercial confidentiality.

Configuration	Tow tension [N]	Winding speed [m/s]
Baseline	nominal	nominal
Configuration 1	2x nominal	nominal
Configuration 2	0.5x nominal	nominal
Configuration 3	nominal	0.5x nominal
Configuration 4	nominal	0.25x nominal

The layup of the vessel is programmed in machine code based on the winding angle. This machine code allows to generate the coordinates of the nominal winding paths, in Euclidean and cylindrical coordinates. These winding paths do not take into account the other manufacturing

parameters that control the winding, such as the winding speed or tow tension (these parameters and encoded in other parts of the machine code), therefore a common set of winding coordinates exist regardless of the vessel configuration. These coordinates form one of the fundamental data used in this methodology.

During winding of the CPVs an initial length of fiber is manually tied around the liner by the operator, afterwards a control arm rotates the entire vessel around the longitudinal axis, such that the fiber wraps around the vessel as it unwinds from the spool(s). To control the winding angle the tows are translated in the longitudinal direction of the vessel. This can be achieved in either of two ways: a guide eye (where all the fiber tows converge at the end of the production line, before being deposited around the vessel) moves in the longitudinal direction of the vessel while the last remains stationary (but rotating). An alternative is for the vessel to be attached to a mechanical arm that translates the entire vessel longitudinally while the guide eye remains stationary. In this work, the vessel is translated by a mechanical arm.

The other necessary data consists of the time signals recorded during the winding of the vessel. These signal are recorded at a rate of 10 Hz, with several signals beyond the scope of this work being recorded. The recorded signals of interest in this work are the following:

- Tow tension;
- Winding speed;
- Length of fiber used.

The vessel is composed of hoop and helical layers. Hoop layers are close to 90° (in relation to the longitudinal axis of the vessel) and are the most load bearing layers. These layers are responsible for constraining the vessel in the radial direction. In contrast, the helical layers are wound with lower angles and are responsible for constraining the vessels in the longitudinal direction and covering the dome sections of the vessel. Each layer is composed of several circuits (a single winding pass over the length of the vessel). Hoop layers are composed of two to three circuits, while helical layers are composed of up to 49 circuits. These two types of layers and winding paths are represented in Figure 2.

3 METHODOLOGY

In the manufacturing setup used in this work, the information about the position of the mechanical arm (and therefore the vessel) is not recorded. This means that we cannot immediately match the coordinates of the winding path to the manufacturing data and it requires additional processing steps to match the manufacturing data to the vessel geometry.

3.1 Matching winding path length to manufacturing winding length

To match these data an alternative method is necessary. Since the fiber length is available from the manufacturing data (Table 2) and we can calculate the vector length (which is equivalent to the fiber used) between each of the coordinates of the winding paths (Table 3), we have a quantity that we can use to match between both sets of data.

However, due to the fact that the winding path is common to all vessels and does not take into account the variations caused by the differences in tow tension and liner pressure (higher tow tension leads to lower amount of fiber required to complete a circuit, and higher liner pressure

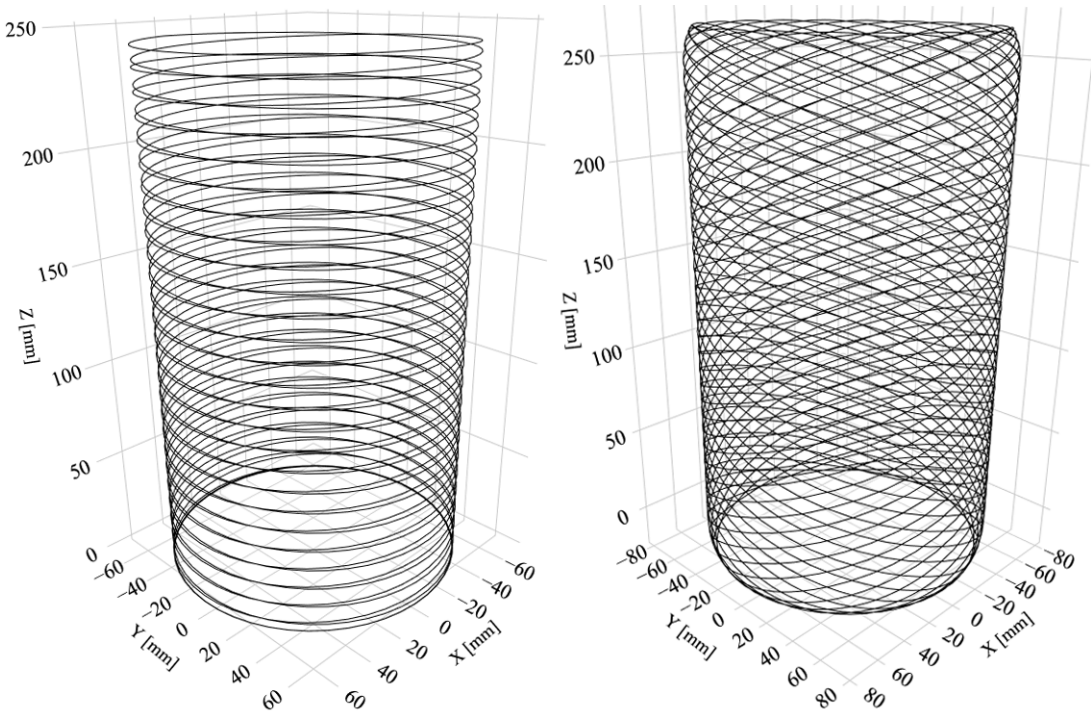

Figure 2: Example of hoop winding paths (left) and helical winding paths (right).

Table 2: Example of the data acquired during winding. Only the relevant parameters are shown.

Time step [s]	Tow tension [N]	Winding speed [m/s]	Used fiber [m]
0.0	T_1	S_1	0.0
t_2	T_2	S_2	L_2
t_3	T_3	S_3	L_3
...	...	...	...
t_m	T_m	S_m	L_m

Table 3: Example of the winding path parameters. Cylindrical coordinates are also recorded but not required. Vector length is calculated *a posteriori*.

X pos. [mm]	Y pos. [mm]	Z pos. [mm]	Vector length [mm]
X_1	Y_1	Z_1	0.0
X_2	Y_2	Z_2	$\sqrt{(X_2 - X_1)^2 + (Y_2 - Y_1)^2 + (Z_2 - Z_1)^2}$
X_3	Y_3	Z_3	$\sqrt{(X_3 - X_2)^2 + (Y_3 - Y_2)^2 + (Z_3 - Z_2)^2}$
...	...	...	...
X_n	Y_n	Z_n	$\sqrt{(X_n - X_{n-1})^2 + (Y_n - Y_{n-1}1)^2 + (Z_n - Z_{n-1})^2}$

leads to higher amount of fiber being necessary), we need to perform corrections to the winding coordinates to properly match these data.

During the winding of the vessel it can be empirically observed that when the winding reaches

one edge of vessel the winding speed drastically reduces to allow a change of direction of the robotic arm in the opposite direction to begin the next circuit. We can leverage this knowledge to match each circuit's local maximum longitudinal position (Z coordinate, which corresponds to a change in the direction of the robotic arm) to the corresponding speed valley detected in the winding speed (which correspond to a point when the winding reached one edge of the vessel). This procedure is illustrated in Figure 3 for hoop layers and Figure 4 for helical layers. Figure 5 shows the same matching procedure for helical layers for a reduced number of circuits.

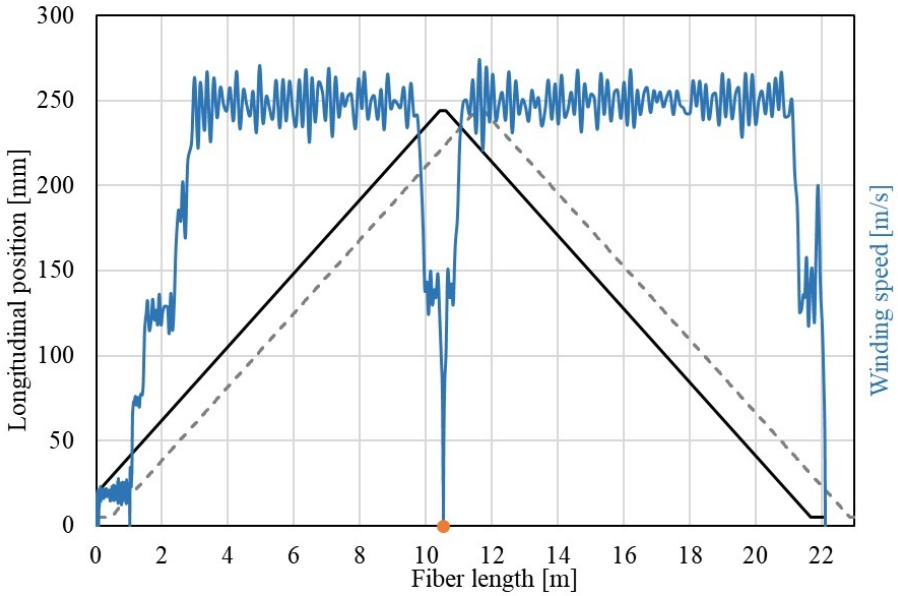

Figure 3: Matching procedure for hoop layers. The original winding path (dashed line) is moved such that the maximum point (change in longitudinal direction) matches the speed valley (change in winding direction). Speed values are omitted due to confidentiality

When the used fiber length datapoints are matched between both sets of data we can interpolate the Euclidean coordinates from the winding paths onto the manufacturing datapoints and reconstruct a 3D plot of the relevant winding parameters (winding speed and tension) over the geometry of the vessel. This mapping is then used to reconstruct the manufacturing parameter's field through Gaussian regression (also called Kriging).

3.2 UV mapping and Gaussian regression

To allow the data to be used as input for ML algorithms (such as Convolutional Neural Networks) it is typically necessary to represent the mapping in 2D space (UV space). However, to maintain the continuity of the regression field as a two-dimensional representation of a cylindrical space it is necessary to perform the Gaussian regression from the 3D space, then unwrap the prediction grid into 2D space. This will also allow to perform data augmentation by shifting the U axis origin of the 2D mapping, since this represents an arbitrary position of the UV mapping over the cylindrical surface. This UV mapping is performed using Eq. 1, where X, Y, Z represent the 3D Euclidean coordinates of the manufacturing datapoints.

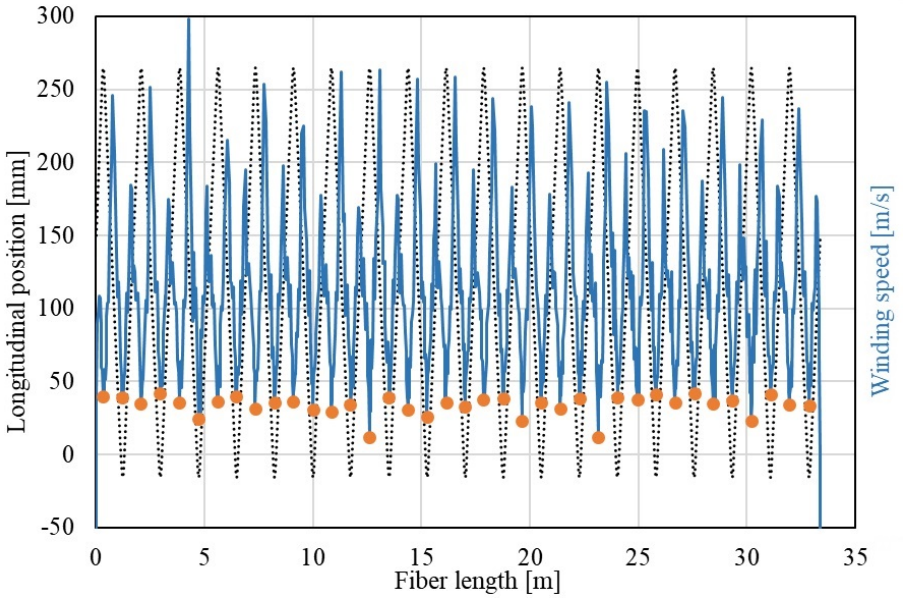

Figure 4: Matching procedure for helical layers. The procedure is the same as for hoop layers, but for a larger number of circuits. Speed values are omitted due to confidentiality.

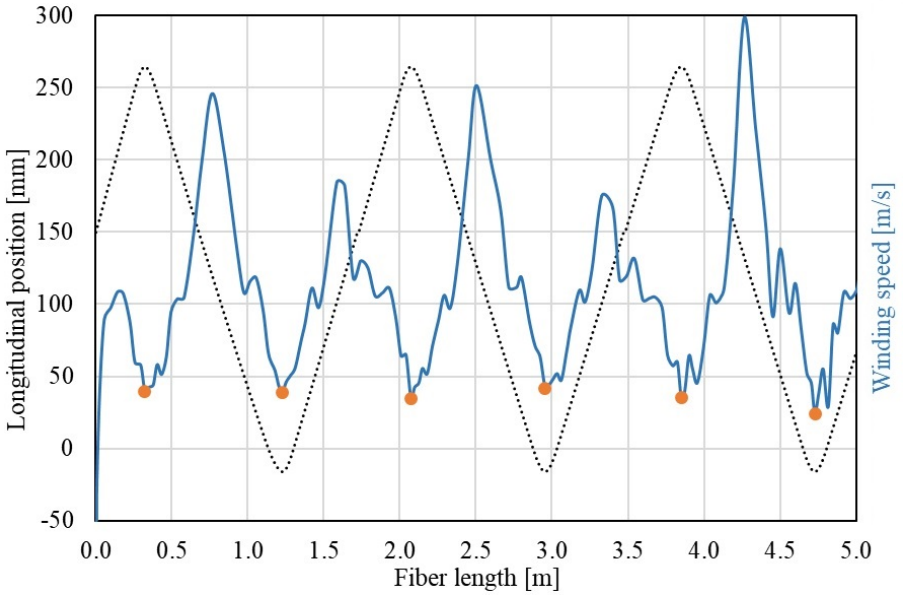

Figure 5: Detail of the matching procedure for helical layers, showing a reduced number of circuits. Speed values are omitted due to confidentiality

$$U = \arctan 2(Y, X); V = Z \tag{1}$$

Gaussian Process Regression (GPR) is a non-parametric probabilistic model widely used in machine learning and statistical analysis [11]. Gaussian Regression allows for predictions

in regression models and uncertainty estimation of the regression model. Unlike traditional regression models that rely on fixed parametric forms, GPR uses prior distributions that are defined by the choice of kernel (covariance function).

To perform Gaussian regression a Matérn kernel is used. This is a general kernel that is often used when few assumptions about the from of the underlying data can be made. This kernel's form is shown in Eq. 2, where $d(x_i, x_j)$ represents the Euclidean distance between every possible pair of points, $K_\nu(\cdot)$ is a modified Bessel function and $\Gamma(\cdot)$ is the gamma function. The value nu controls the smoothness of the generated functions. A value of 1.5 was used. The value l is called the correlation length, and it controls how far in the input space the points are correlated with each other. This can be a single value (called an isotropic kernel), where the correlation length is the same in all directions, or a vector (called an anisotropic kernel), where the value can be different in each direction. An anisotropic kernel was used, and the value of l is optimized through the maximization of the likelihood.

$$k(x_i, x_j) = \frac{1}{\Gamma(\nu)2^{\nu-1}}\left(\frac{\sqrt{2\nu}}{l}d(x_i, x_j)\right)^{\nu} K_\nu\left(\frac{\sqrt{2\nu}}{l}d(x_i, x_j)\right) \tag{2}$$

4 RESULTS AND DISCUSSION

Following the procedure elaborated in the Methodology, we matched the winding path data to the manufacturing data of a hoop layer (the first hoop layer) and a helical layer of a vessel with nominal configuration.

The procedure of matching the winding path data to the manufacturing data is illustrated in Figures 3 to 5. After the matching procedure, the winding path coordinates are interpolated into the existing manufacturing length datapoints and used to reconstruct a 3D mapping of the manufacturing data.

Figure 6 shows the winding parameter's (winding speed and tow tension) mapping to the geometry of a hoop layer. Here, it can be observed the initial length of fiber that was tied-in by the operator as concentration of points with lower winding speed at the base of the vessel. This is verified by empirical observations, as this portion of the vessel is wound at a lower speed. In the winding speed mapping we can also observe at the top edge of the vessel points with lower winding speed. This mapping confirms that the winding starts at the bottom edge and proceeds to the top edge, where the winding changes direction and the next circuit begins. Figure 6(b) shows a more uniform distribution of the tow tension for a hoop layer, but we can still observe points of higher and lower tension around the top and bottom edges of the vessel. We can attribute these to a delay in the tension control of the production line: as the winding approaches the edge of the vessel the radius changes slightly and this requires an adjustment of the tension control system to compensate for this deviation. However, a slight delay in the control system leads to momentary over- and under-tension of the fibers around the edges.

We then perform the UV mapping and Gaussian regression of these mappings. These can be seen in Figures 7 and 8 for the winding speed and winding tension, respectively. From these we can observe the Gaussian regression of the speed field preserves more of the anisotropy that we would expect from the direction of the winding, but both conform well to their respective UV mapping.

The same procedure is then repeated for a helical layer, with the results shown in Figures 9

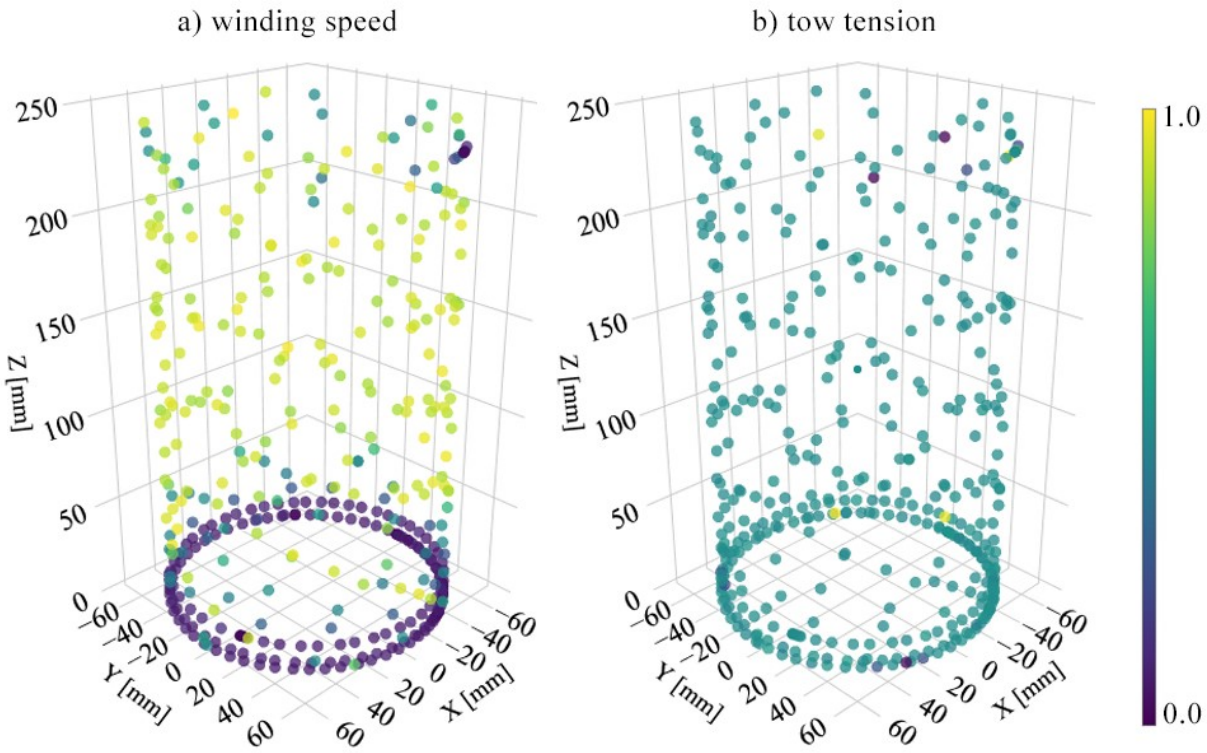

Figure 6: Hoop layer datapoints represented in 3D space after interpolation of the manufacturing datapoints to the matched winding path. a) Normalized winding speed values. b) Normalized tow tension values. Values where normalize due to commercial confidentiality.

to 11. The same observations can be made for the helical layers: we see a higher winding speed in the middle of the vessel (this is corroborated by empirical observations) and more extreme values of tension at the edges of the vessel. In Figure 10 we can also see some points with lower winding speed in the middle of the vessel. The reason for these can are not obvious, but highlight the importance and usefulness of this method: it allows to detect deviations from the normal winding conditions that would be masked by simply averaging the information in the signal.

5 CONCLUSIONS

In this paper we presented a methodology to map manufacturing variability to the geometry of composite pressure vessels. By recording time signals of relevant manufacturing parameters during the winding process, and matching these signals to the winding paths resultant from defining the winding angles of each layer, we produced a mapping of the winding speed and tow tension over the vessel's surface. Gaussian Regression was then applied to these maps to generate continuous fields of these parameters, highlighting the spatial variability of these parameters.

This approach provides valuable insights into the distribution of the manufacturing parameter's variability in composite pressure vessels, which is critical for predicting the performance (burst pressure) and identifying potential critical areas of the vessel. The mapping and regression techniques developed in this work can be used to generate input data with uncertainty infor-

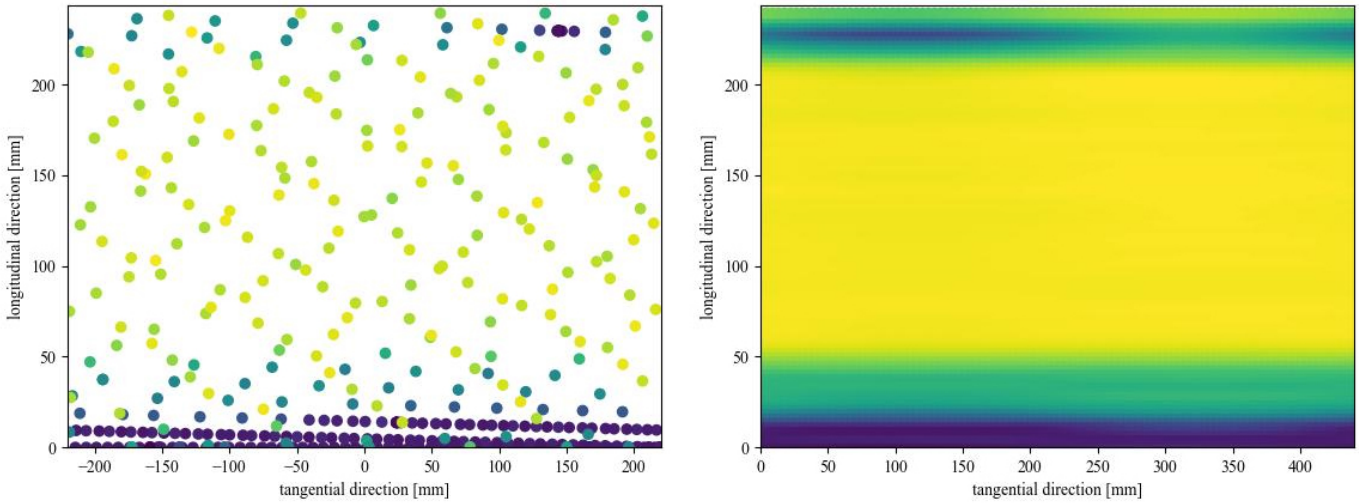

Figure 7: Hoop layer UV mapping of the winding speed (left) and corresponding Gaussian regression of the winding speed field (right).

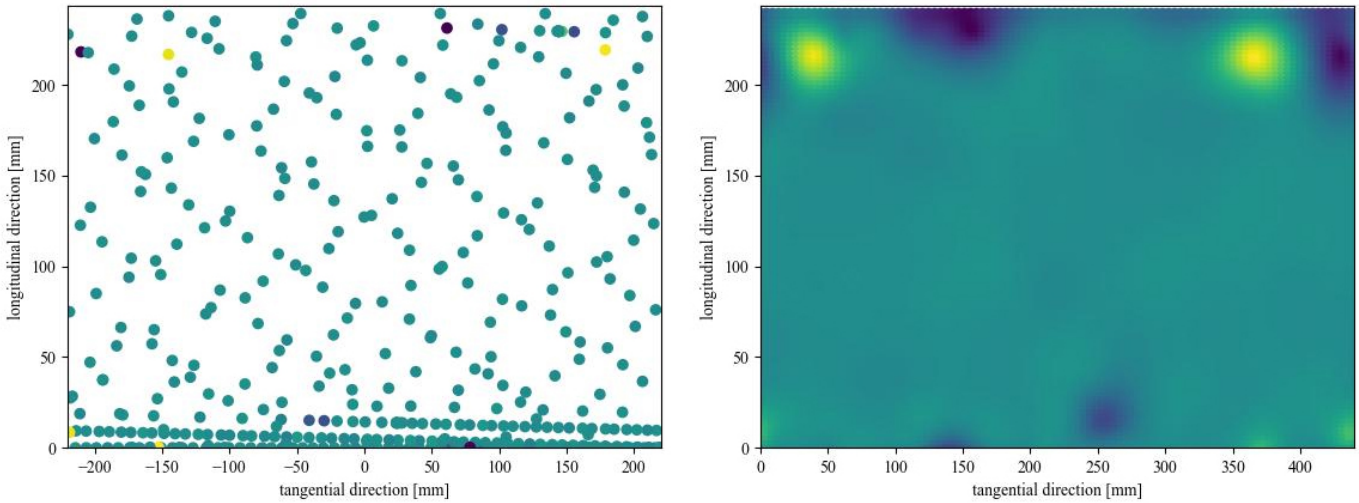

Figure 8: Hoop layer UV mapping of the winding tension (left) and corresponding Gaussian regression of the winding tension field (right).

mation for machine learning models aimed at predicting burst pressure and other performance metrics of CPVs.

Future work will focus on continuing this methodology, using the generated mappings as inputs to convolutional neural networks for prediction of the burst pressure of CPVs.

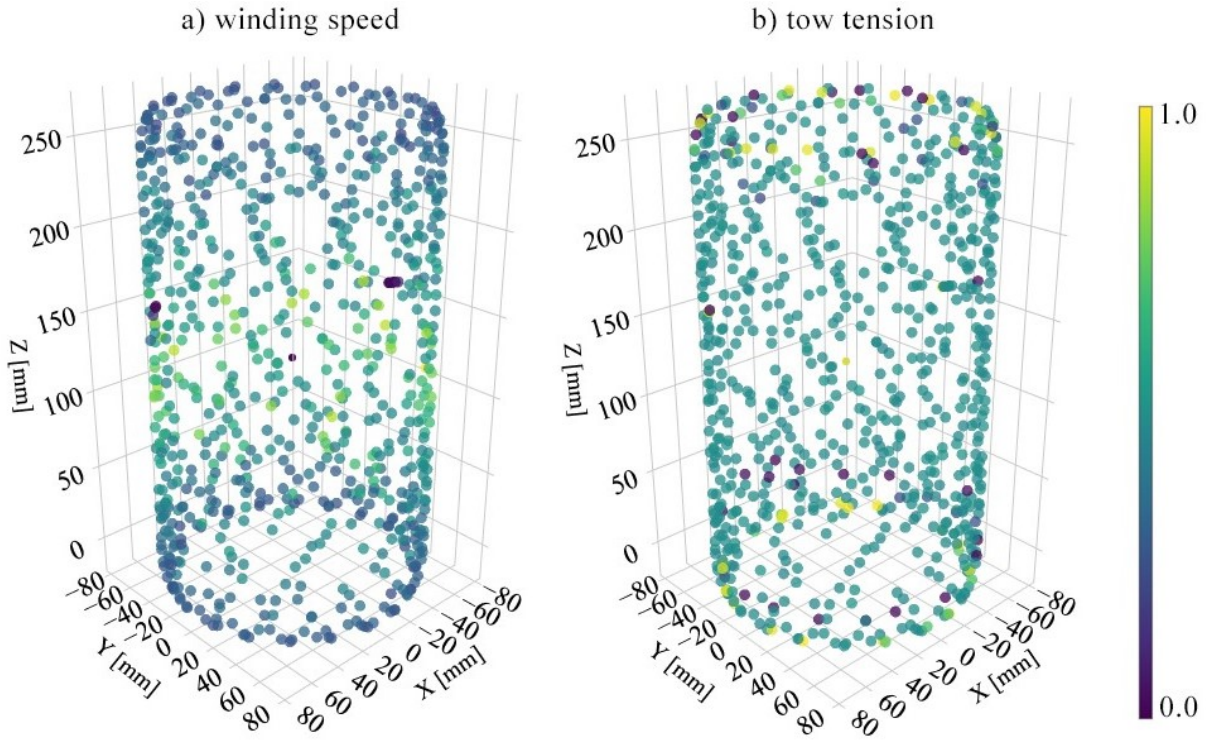

Figure 9: Helical layer datapoints represented in 3D space after interpolation of the manufacturing datapoints to the matched winding path. a) Normalized winding speed values. b) Normalized tow tension values. Values where normalize due to commercial confidentiality.

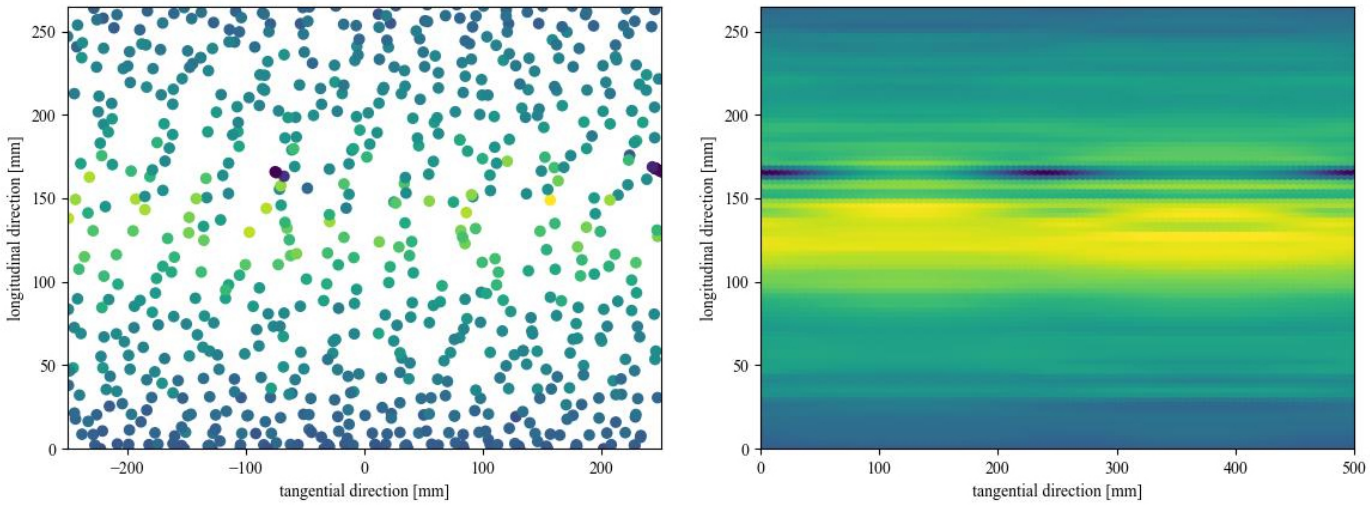

Figure 10: Helical layer UV mapping of the winding speed (left) and corresponding Gaussian regression of the winding speed field (right).

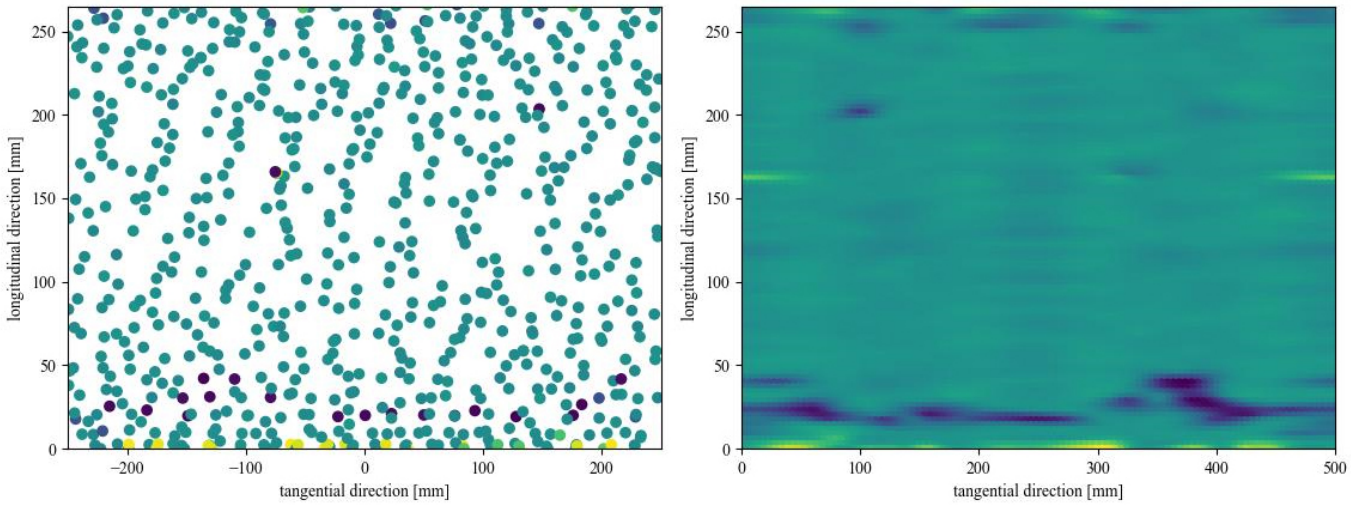

Figure 11: Helical layer UV mapping of the winding speed (left) and corresponding Gaussian regression of the winding speed field (right).

ACKNOWLEDGMENTS

The authors gratefully acknowledge the SIM (Strategic Initiative Materials in Flanders) NanoForce program and VLAIO (Flanders Innovation & Entrepreneurship Agency) for their financial support through the OptiVaS project.

REFERENCES

[1] Air, A., Shamsuddoha, M., and Gangadhara Prusty, B. A review of type v composite pressure vessels and automated fibre placement based manufacturing. 110573.

[2] American Society of Mechanical Engineers. *BPVC Section X-Fiber-Reinforced Plastic Pressure Vessels*. ASME.

[3] Dwivedi, N., and Kumar, V. Burst pressure prediction of pressure vessel using FEA.

[4] Dwivedi, N., Kumar, V., Shrivastava, A., and Nareliya, R. Burst pressure assessment of pressure vessel using finite element analysis: A review.

[5] Fryer, D. M., and Harvey, J. F. High pressure vessels. In *High Pressure Vessels*, D. M. Fryer and J. F. Harvey, Eds. Springer US, pp. 1–10.

[6] Harada, S., Arai, Y., Araki, W., Iijima, T., Kurosawa, A., Ohbuchi, T., and Sasaki, N. A simplified method for predicting burst pressure of type III filament-wound CFRP composite vessels considering the inhomogeneity of fiber packing. 79–90.

[7] Johnson, W. R., Zhu, X.-K., Sindelar, R., and Wiersma, B. A parametric finite element study for determining burst strength of thin and thick-walled pressure vessels. 104968.

[8] Ladokun, T., Nabhani, F., and Zarei, S. Accidents in pressure vessels: Hazard awareness. In *Proceedings of the World Congress on Engineering 2010*, vol. Vol II.

[9] Rafiee, R., and Salehi, A. A novel recursive multi-scale modeling for predicting the burst pressure of filament wound composite pressure vessels. 388.

[10] Rafiee, R., and Torabi, M. A. Stochastic prediction of burst pressure in composite pressure vessels. 573–583.

[11] Rasmussen, C. E., and Williams, C. K. I. *Gaussian processes for machine learning*. Adaptive computation and machine learning. MIT Press. OCLC: ocm61285753.

[12] Sloan, J. Composites end markets: Pressure vessels (2023). https://www.compositesworld.com/articles/composites-end-markets-pressure-vessels-2023.

[13] Zolfaghari, A., and Izadi, M. Burst pressure prediction of cylindrical vessels using artificial neural network.